

Neural network based direct torque control for doubly fed induction generator fed wind energy systems

Aftab Ahmed Ansari* and Giribabu Dyanamina^a

*Department of Electrical Engineering, Maulana Azad National Institute of Technology,
Link Road Number 3, Near Kali Mata Mandir, Bhopal, Madhya Pradesh, 462003, India*

(Received December 17, 2021, Revised May 12, 2023, Accepted May 15, 2023)

Abstract. Torque ripple content and variable switching frequency operation of conventional direct torque control (DTC) are reduced by the integration of space vector modulation (SVM) into DTC. Integration of space vector modulation to conventional direct torque control known as SVM-DTC. It had been more frequently used method in renewable energy and machine drive systems. In this paper, SVM-DTC is used to control the rotor side converter (RSC) of a wind driven doubly-fed induction generator (DFIG) because of its advantages such as reduction of torque ripples and constant switching frequency operation. However, flux and torque ripples are still dominant due to distorted current waveforms at different operations of the wind turbine. Therefore, to smoothen the torque profile a Neural Network Controller (NNC) based SVM-DTC has been proposed by replacing the PI controller in the speed control loop of the wind turbine controller. Also, stability analysis and simulation study of DFIG using process reaction curve method (RRCM) are presented. Validation of simulation study in MATLAB/SIMULINK environment of proposed wind driven DFIG system has been performed by laboratory developed prototype model. The proposed NNC based SVM-DTC yields superior torque response and ripple reduction compared to other methods.

Keywords: direct torque control; doubly fed induction generator; neural network controller; rotor side converter; space vector modulation; wind turbine

1. Introduction

The fast depletion of fossil fuels and the impact of extensive use of natural resources on the mother nature led to numerous research studies to use alternative sources such as solar, wind, and tidal for electrical power generation. Out of these wind energy and solar energy are contemporary technologies serving the increasing global energy demand. Wind energy is most extensively used across the globe due to its bulk production capability compared to solar energy (Global Wind Report 2022 - Global Wind Energy Council, n.d.). A wind energy system (WES) is designed with a wind turbine, gear box, generator, power electronic converter, control system, and grid interfacing unit. Wind turbines are divided into constant and variable speed turbines further upon the generators used variable speed turbines are again divided into partial variable speed (10% and 30%) and fully variable speed (100%) (Yamasu *et al.* 2015, Ansari and Dyanamina 2022b). The

*Corresponding author, Ph.D. Student, E-mail: aftab786zakir@gmail.com

^a Ph.D., Professor, E-mail: dgiribabu208@gmail.com

type of generator plays a critical role in deciding the range of speed operation, namely squirrel-cage induction generator (SCIG) (Nguyen and Lee 2022), doubly-fed induction generator (DFIG) (Ansari and Dyanamina 2022a, Ansari *et al.* 2021) and the permanent magnet synchronous generators (PMSG) (Zheng *et al.* 2021). DFIG is the most suitable machine for partial variable-speed operation WES, in these, the stator terminals of the machine are connected to the utility grid such that its frequency is constant, whereas rotor terminals are connected to the grid through power electronic converters connected back to back converter which converts AC-DC and DC-AC through buffer capacitor. The partial variable speed operation i.e. $\pm 30\%$ of the rated speed in DFIG is possible through a Machine or Rotor Side Converter (RSC), Load, or Grid Side Converter (GSC) with an intermediate DC voltage link. This property of DFIG makes it most economical compared to SCIG and synchronous generator based WES. Controlling of the power converters allows the DFIG to extract maximum energy during a change in wind speed (Gupta and Dyanamina 2019, Conchas *et al.* 2023).

Vector control is employed to independently control the active and magnetizing power of the generator through stator or rotor flux orientation using a speed sensor (Ansari and Dyanamina 2022a). The pros of this method are less power ripple, lower converter switching frequency, and high dynamic response but this control method suffers from performance variation due to changes in machine parameters and critical online computation for generating gate pulses (Pena *et al.* 1996, Ansari *et al.* 2023). Apart from VC alternative techniques for instance direct torque control (DTC) (Takahashi and Noguchi 1986, Muyeen *et al.* 2009), and direct power control (DPC) (Takahashi and Noguchi 1986, Sahri *et al.* 2021) were also introduced to enhance the performance of wind system. The elimination of the outer speed control loop in the DTC of the WES makes its control simpler compared to the VC, where the torque is estimated from the machine. DTC offers advantages such as absence of parameter dependency and coordinate transformation compared to VC but it has limitations such as changeable switching frequency and more torque ripples may also reduce the operational life of the turbine and generate more noise (Patel and Dyanamina 2017). During low wind speeds performance of WES is poor and contains more ripples in DC link voltage, therefore a new method combining vector and DTC, known as the hybrid control method was introduced, to reduce the torque ripples by combining the advantages of both methods in (Mohammadi *et al.* 2018), though ripple content is reduced, implementation of hybrid method is a tedious task at variable speeds. The predictive torque control approach presented in the literature (Mossa *et al.* 2019, Sguarezi Filho, 2022) to reduce the limitations of the conventional DTC both at steady state and transient state operation. SVM is integrated into conventional DTC to enhance the performance of the DFIG, particularly to reduce torque ripples and for constant frequency operations (Gupta and Dyanamina 2019).

A sliding mode controller (SMC) based transient performance improvement method for DFIG based wind energy system was proposed. In this, SMC is employed to enhance the dynamic performance of the wind system at various wind speeds. Implementation of SMC in the DTC results in improved transient response, boundary computation during stability analysis of the SMC is critical for DFIG based WES (Jaladi and Sandhu 2018). In this paper, a neural network-based DTC method has been proposed to reduce the torque and flux ripples. The implementation of NNC improves the transient torque response and integration of SVM to NNC based DTC yields more power output at variable wind speeds. The paper is organized into different sections, where section 1 comprises of literature review, section 2 presents about the modelling of a wind turbine, section 3 discusses about the mathematical modelling of DFIG, section 4 presents the explanation of the DTC method and stability analysis using PRC method, section 5 presents the implementation of

SVM to DTC method, section 6 discuss about the neural network controller and its implementation, section 7 presents development and implementation of prototype model using digital controller and results and discussions at different wind speeds and section 8 presents the conclusion.

2. Mathematical modelling of wind turbine model

The mechanical power produced by the wind turbine is expressed as:

$$P_m = .5C_p V_w^3 \pi R^2 \rho \quad (1)$$

From a wind turbine the torque input fed to DFIG is represented as:

$$T_g = \frac{(.5C_p \rho \pi R^2 V_w^3)}{\omega_m} \quad (2)$$

Expression for maximum power coefficient at an optimum value of tip speed ratio λ is written as:

$$C_p(\lambda, \beta) = .5176 \left(\left(\frac{116}{\lambda} \right) - .4\beta - 5 \right) e^{(-21/\lambda)} + .0038\lambda \quad (3)$$

The above equation is rewritten as:

$$\frac{1}{\lambda} = \frac{(1)}{(\lambda + .08\beta)} - \frac{(.035)}{(1 + \beta^3)} \quad (4)$$

2.1 Modeling of DFIG

The motoring rule is used for the mathematical analysis, where the currents entering the network, real and reactive powers are assigned negative signs when they enter the power network. The mathematical expression of the DFIG employed for wind power generation expressed in the d-q axis with synchronous reference frame is written as (Abad *et al.* 2011, Ansari *et al.* 2021):

$$u_{ds} = R_s i_{ds} + \frac{d\phi_{ds}}{dt} - \omega_s \phi_{qs} \quad (5)$$

$$u_{qs} = R_s i_{qs} + \frac{d\phi_{qs}}{dt} - \omega_s \phi_{ds} \quad (6)$$

$$u_{dr} = R_r i_{dr} + \frac{d\phi_{dr}}{dt} - (\omega_s - \omega_r) \phi_{qr} \quad (7)$$

$$u_{qr} = R_r i_{qr} + \frac{d\phi_{qr}}{dt} - (\omega_s - \omega_r) \phi_{dr} \quad (8)$$

The d-q axis flux linkages produced are expressed as:

$$\phi_{ds} = (L_{ls} + L_m) i_{ds} + L_m i_{dr} \quad (9)$$

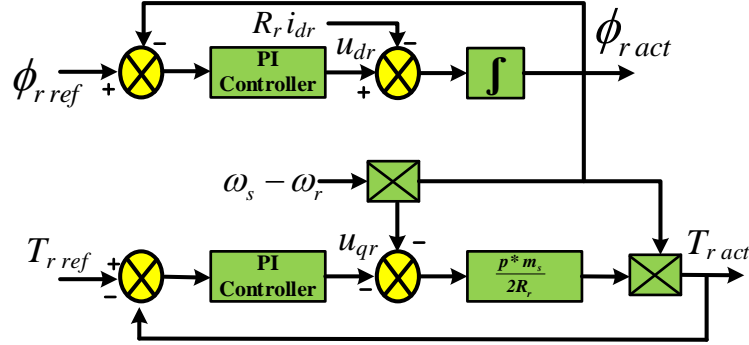


Fig. 2 Control loop for flux and torque controller

and magnetizing powers. The illustrative model of the SVM-DTC is shown in Fig. 1. It consists of three loops; the first is the flux loop, the second is the torque loop, and the last is the speed loop. In the flux control loop, initially, actual rotor flux of the machine is determined, which is compared with reference flux and the error value is provided as input to the PI controller to produce d – axis rotor voltage as the output of the controller. Similarly in the torque loop actual electromagnetic torque is determined initially and is compared with reference torque, the torque error is provided as input to the PI controller to produce q – axis rotor voltage as output. Finally, the speed control loop consists of a neural network controller whose input is speed error from actual and reference speeds and produces the torque reference to the second controller (Gupta and Dyanamina 2019, Benbouhenni and Bizon 2021).

3.1 Stability study using process reaction curve method

To obtain the transfer function of the electromagnetic torque and rotor flux the voltage drop across rotor resistance and linkage between torque and flux is also neglected. The rotor side converter switches delay is included for analysis. The block diagram of a mathematical model of flux and torque control loops is illustrated in Fig. 2. By The transfer function using Eqs. (5) - (12) is written as (Jaladi and Sandhu 2018):

$$\begin{aligned} & \left(R_s L_r - \frac{(k k_1 R_s L_r)}{R_r} \frac{d}{dt} \right) u_{dr} \\ &= R_s R_r \phi_{dr} + k_3 \frac{d\phi_{qr}}{dt} - \frac{(R_s L_r k k_1)}{R_r} \frac{d^2 \phi_{dr}}{dt^2} + \frac{(R_s L_r k k_1)(\omega_s - \omega_r)}{R_r} \frac{d\phi_{qr}}{dt} \\ & \quad - (R_s L_r (\omega_s - \omega_r) + R_r L_s \omega_s) \phi_{qr} - (R_s L_r k u_{ds}) - (\omega_s R_s L_r k k_1 i_{qr}) \end{aligned} \quad (18)$$

where $k = \frac{R_r L_m}{R_s L_r}$, $k_1 = \frac{(L_m - L_s L_r)}{L_m}$

By using stator flux orientation q-axis component is zero, so open loop transfer function is given by the below equation:

$$\frac{\Phi_{dr}(s)}{u_{dr}(s)} = \frac{R_s L_r + (L_s L_r - L_m^2) s}{(L_s L_r - L_m^2) s^2 + (R_s L_r + R_r L_s) s + R_s R_r} \quad (19)$$

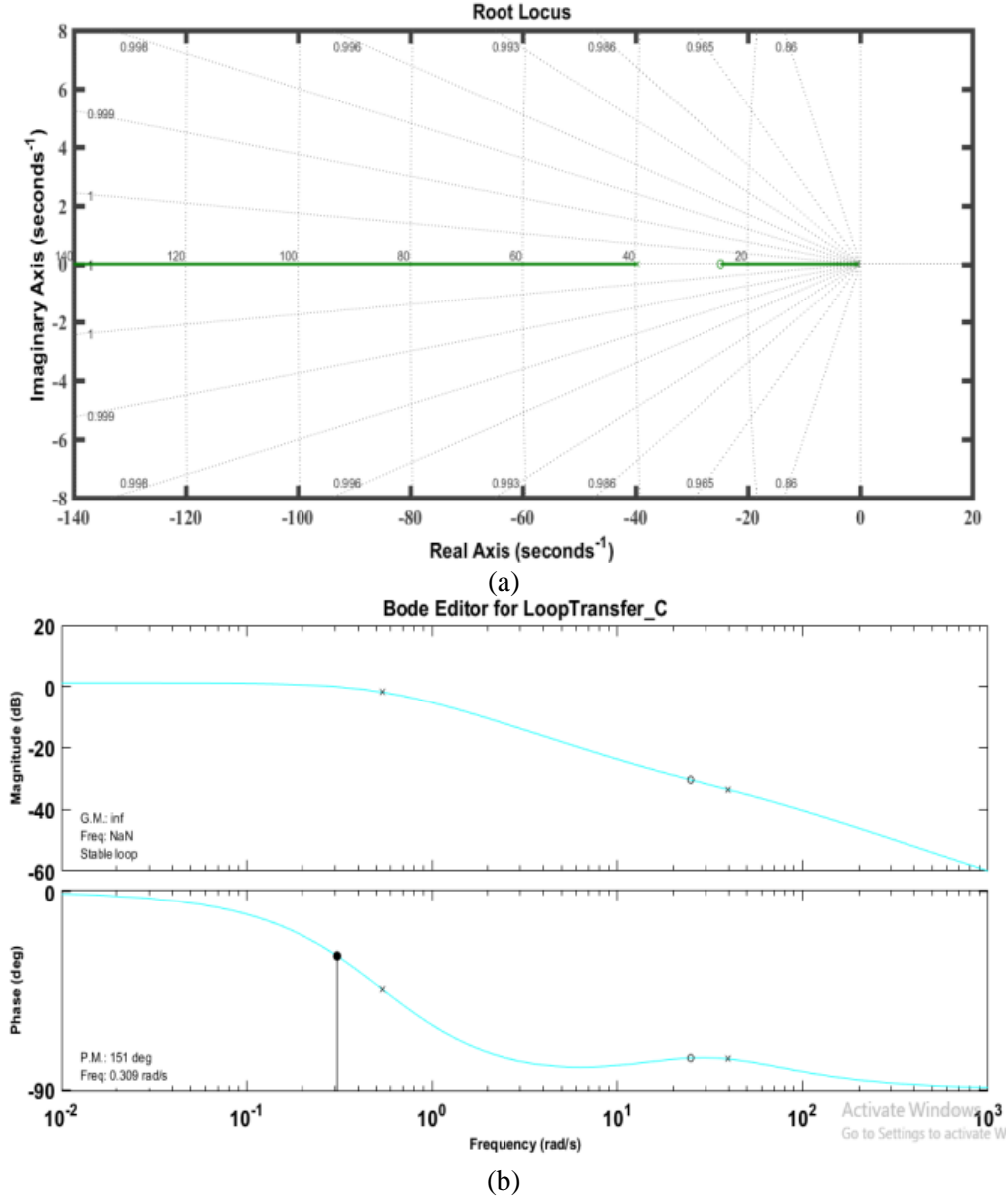
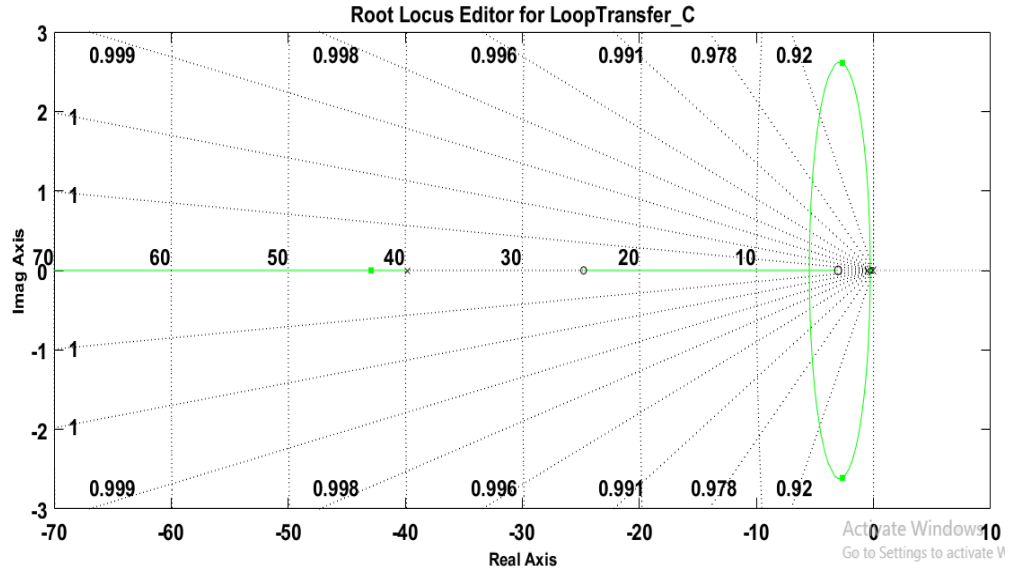


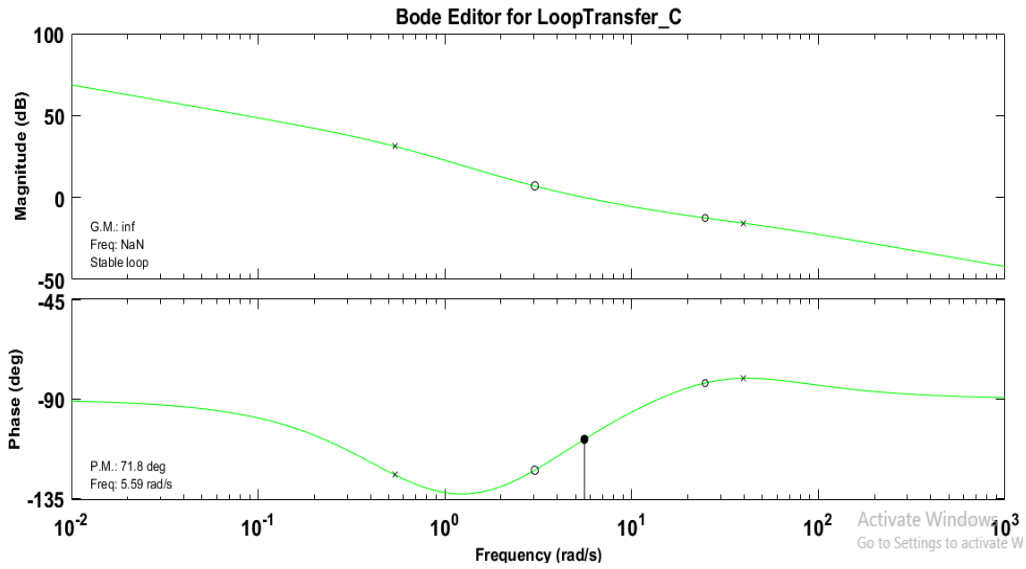
Fig. 3 Root locus and Bode plot of flux controller without PI

$$L_s \frac{du_{qr}}{dt} = \left(k_3 \frac{d}{dt} - k_1 L_m \frac{d^2}{dt^2} \right) i_{qr} + L_s (\omega_s - \omega_r) k_2 \frac{d}{dt} i_{dr} + L_m \frac{du_{qs}}{dt} - R_s \frac{d\phi_{qr}}{dt} - L_s k_2 i_{dr} \frac{d\omega_r}{dt} \quad (20)$$

where $k_2 = \frac{(L_s L_r - L_m^2)}{L_s}$, $k_3 = R_r L_s + R_s L_r$



(a)



(b)

Fig. 4 Root Locus and Bode Plot of flux controller with PI

Using Eq. (15), and considering stator flux orientation then i_{qr} and $\frac{d\omega_r}{dt}$ is calculated as:

$$i_{qr} = -\frac{(2L_s T_e)}{3pL_m \phi_{ds}} \quad (21)$$

$$\frac{d\omega_r}{dt} = \frac{-3pL_m \phi_{ds} i_{qr}}{2JL_s} \quad (22)$$

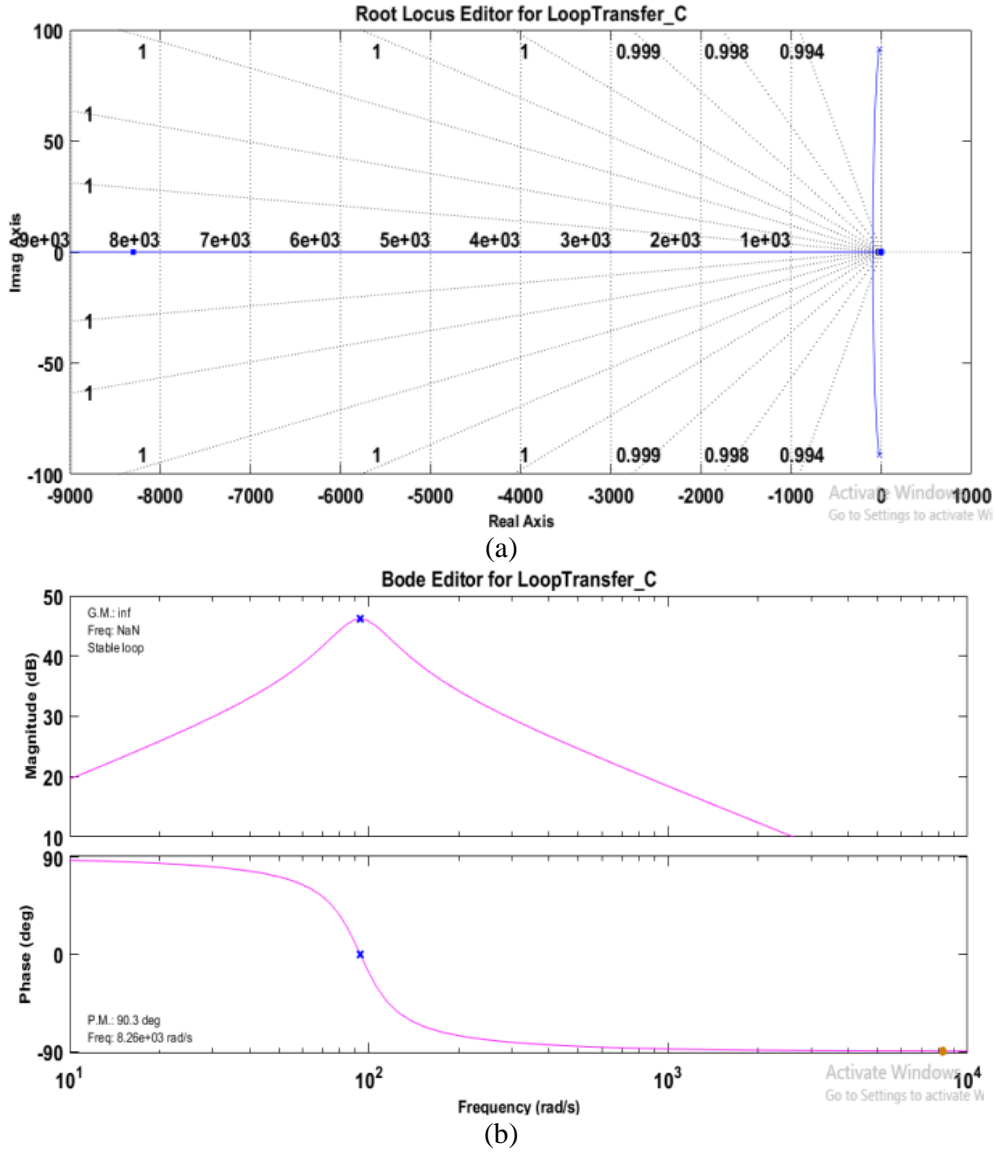


Fig. 5 Root locus and Bode Plot of torque control without PI

Substitute Eqs. (21) and (22) in (20) and multiply with minus one to torque gives the open loop transfer function

$$\frac{T_e(s)}{u_{qr}(s)} = \frac{sL_s}{\frac{2L_s}{3p\phi_{ds}} \left(\frac{(L_s L_r - L_m^2)}{L_s} \right) s^2 + \frac{(2L_s k_3)}{3pL_m \phi_{ds}} s + \frac{pL_m \phi_{ds}}{J}} \quad (23)$$

For stability study of the Eqs. (19) and (23), the uniformity rule technique using SISOTOOL is employed. Root locus, bode plot, and step response without or with PI controller are shown in Fig. 3 to Fig. 6.

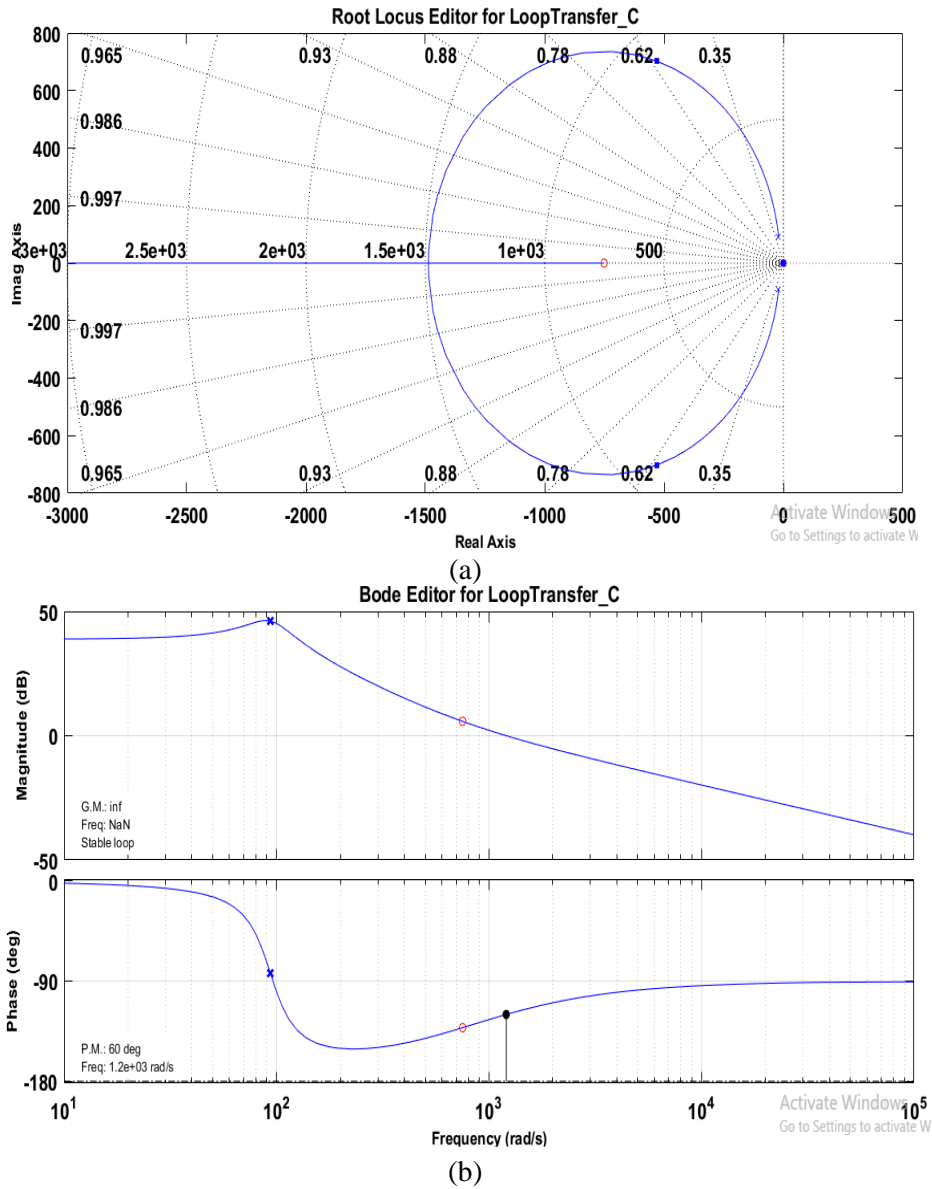


Fig. 6 Root locus and Bode Plot of torque controller with PI

4. Space vector PWM method

The power electronic converter in RSC consists of eight switches, by using these switches, eight voltage vectors are generated and these vectors are stationary. From eight vectors, six vectors are active vectors i.e., u_1 to u_6 form a hexagon shape. The remaining two vectors are zero vectors i.e., u_0 and u_7 are presented at the hexagon center which is shown in Fig. 7. SVM method injects a third harmonic component in the fundamental waveform and the fundamental output increase by 15% as compared to sinusoidal pulse width modulation.

4.1 Dwell time computation

At different switching states of space vectors voltage values are different for balanced conditions therefore three-phase voltages are

$$u_{A0}(t) + u_{B0}(t) + u_{C0}(t) = 0 \quad (24)$$

where u_{A0}, u_{B0}, u_{C0} instantaneous voltages and Space vector representation are is given as:

$$\vec{u}(t) = \mathbf{u}_\alpha(t) + j\mathbf{u}_\beta(t) \quad (25)$$

$$\vec{u}(t) = \frac{2}{3} [\mathbf{u}_{A0}(t)e^{j0} + \mathbf{u}_{B0}(t)e^{j\frac{2\pi}{3}} + \mathbf{u}_{C0}(t)e^{j\frac{4\pi}{3}}] \quad (26)$$

The reference voltage is calculated by taking three nearby stationary vectors. This computation is using volt-second (V-S) equilibrium theory. In this, the reference voltage and sampling time is multiplied and equated to the product of the sum of the product of the time interval and voltages of the selected space vector of the triangle. For instance, if the reference voltage is in the sector – I then the reference voltage is calculated by $\mathbf{u}_1, \mathbf{u}_2, \mathbf{u}_3$ as shown in Fig. 7. The generalized dwell time expression for six sectors of a hexagon is given as:

The expression for V-S balance along α axis:

$$\mathbf{u}_1 T_1 + \mathbf{u}_2 \cos(60) T_2 = \mathbf{u}_{\text{ref}} T_s \cos \theta_r \quad (27)$$

V-S balance along axis:

$$\mathbf{u}_2 \sin(60) T_2 = \mathbf{u}_{\text{ref}} T_s \sin(\theta_r) \quad (28)$$

From Eqs. (27)-(28), T_1, T_2, T_0 are calculated by given below equation:

$$T_1 = \frac{\mathbf{u}_{\text{ref}} T_s \sin(60 - \theta_r)}{U_{\text{dc}} \sin(60)} \quad (29)$$

$$T_2 = \frac{\mathbf{u}_{\text{ref}} T_s \sin(\theta_r)}{U_{\text{dc}} \sin(60)} \quad (30)$$

$$T_0 = T_s - T_1 - T_2 \quad (31)$$

From Eqs. (29)-(31) dwell times for all sectors are calculated, where T_s = sampling time period, U_{dc} = reference dc voltage, θ_r = rotor position angle.

5. Neural network based SVM-DTC

The PI controller in the speed control loop is replaced with a neural network controller. This NNC consists of three layers used to characterize a nonlinear function. These are designated as the input layer, output layer, and hidden layers. Each layer consists of a small internal element known as neurons; the neurons in the hidden layer decide the accuracy of the estimation of the output layer. The output of a NNC is reference torque; it is computed from a (2-16-1) neuron's multilayer feed-forward NN. The speed NNC is simulated as speed error as the input layer and better estimation accuracy is obtained with previous values, whereas it needs a huge amount of training data and enormous computational tries to generate the perfect and precise output (Babaei *et al.*

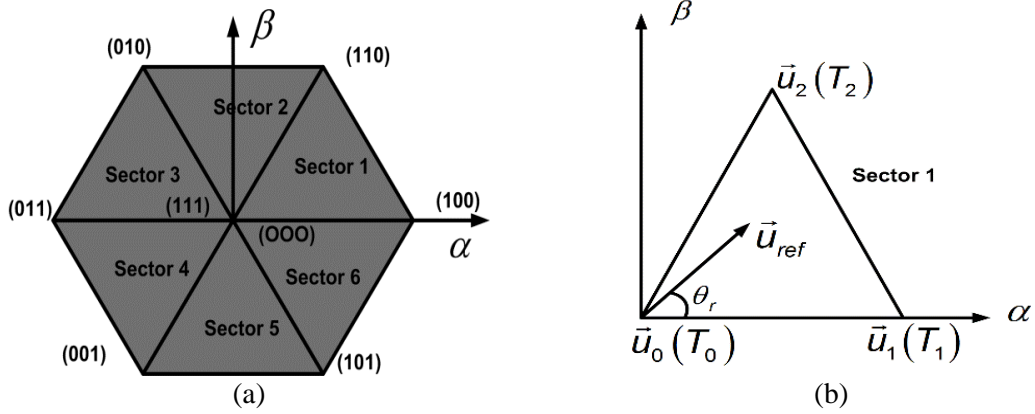
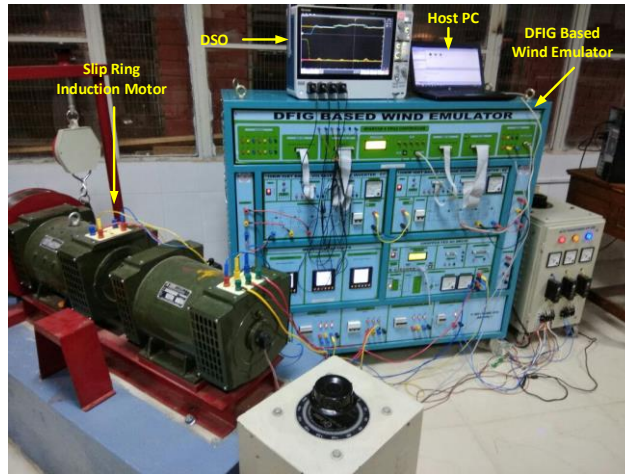
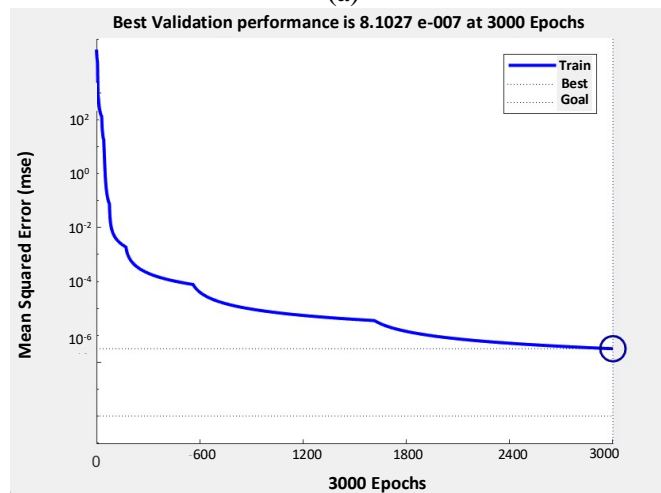


Fig. 7 SVM diagram of space vectors and Dwell time calculation



(a)



(b)

Fig. 8 (a) Prototype model of Wind Energy System (b) Neural Network training algorithm

2022). The simple optimization practice is employed to fine-tune and minimize the weight of neurons, especially the gradient descent technique (GDT), in which the neuron weights are repetitively commencing from the regressive output layer. For a speed NNC output neuron expression is written as:

$$E_m = (d^m - y^m)^2 = \sum_{n=1}^K (d_n^m - y_i^m)^2 \quad (32)$$

From the above equation, the exact output of the n^{th} neuron is d_n^m in the output layer of speed NNC and its analogous actual output is y_n^m , for this actual output, its vector is K, and the equivalent preferred output vector is d^m . For the set of M pattern, the total sum of squared error (SSE) is expressed as:

$$SSE = E = \sum_{m=1}^M E_p = \sum_{m=1}^M \sum_{n=1}^K (d_n^m - y_i^m)^2 \quad (33)$$

The weights of the neurons are altered to obtain the final value of the target function of SSE using GDT. The updated expression of the weight function is:

$$W_{in}(k+1) = W_{in}(k) - \eta \left(\frac{\delta E_m}{\delta W_{in}(k)} \right) \quad (34)$$

where η is called as the learning rate.

A new weight between i^{th} and n^{th} neuron is written as $W_{in}(k+1)$, and its conforming old weight is $W_{in}(k)$ also for all M training outlines the weights of output neurons are iteratively rationalized, which makes the practice of calculating the output neuron accurate as the attained signals contain lesser noise and without harmonics even though WES contains all nonlinearities. Training of NNC of weights up to more than a few hundred, GDT is widely used as it yields training output rapidly and additionally its execution is proficient. For rapid offline training purpose, the Levenberg-Marquardt training process can be used compared to the GDT but it needs huge memory. The training procedure of speed NNC is carried at different operations in MATLAB with ® CoreTM 2 Duo processor operating at 2.94 GHz contains RAM of capacity 4 GB, it persists for about 90 minutes. The speed NNC of DTC is trained with 3000 I/O pattern using mean squared error (MSE) between targets neuron and network, the output deteriorates at a value of 1×10^{-7} subsequently at 3000 epochs as illustrated in Fig. 8(a).

6. Experimental results and discussion

6.1 Prototype development of DFIG graphics

The experimental setup of the proposed wind emulator consists of an inverter model connected to rotor terminals, wound rotor asynchronous machine, dc motor, speed, current and voltage sensors, and dSPACE MicroLabBox R&D controller board. The photograph of the prototype model for experimental validation is illustrated in Fig. 8(b). The real-time implementation of DFIG based WES is performed in the laboratory using dSPACE MicroLabBox consisting of Q or IQ P5020 as the real-time processor. This processor is a new model from dSPACE available as a dual-core system having clock frequency up to 2 GHz and armed with a programmable FPGA (Xilinx

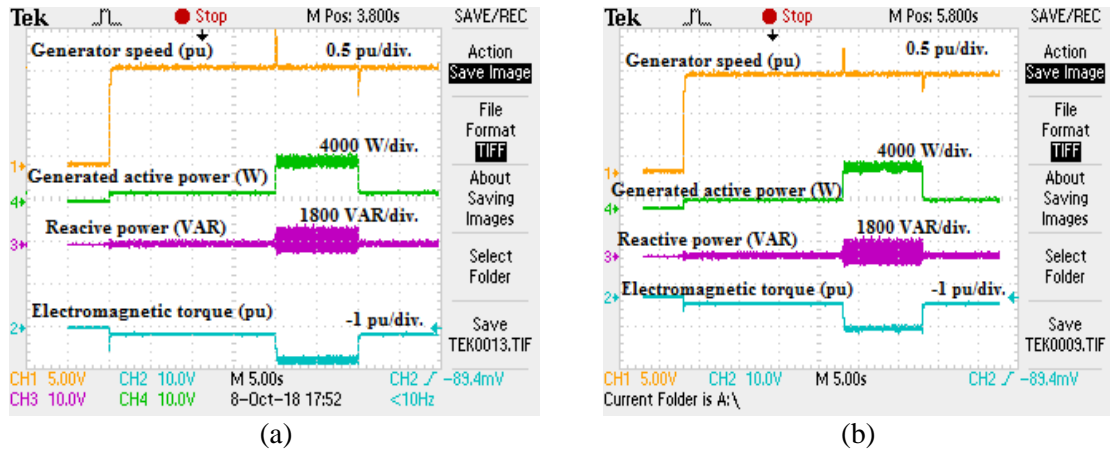


Fig. 9 Comparison of waveforms of Generator speed response (Channel 1), generated active power (Channel 4), and reactive power (Channel 3), electromagnetic torque (Channel 2) using (a) PIC and (b) NNC based SVM-DTC

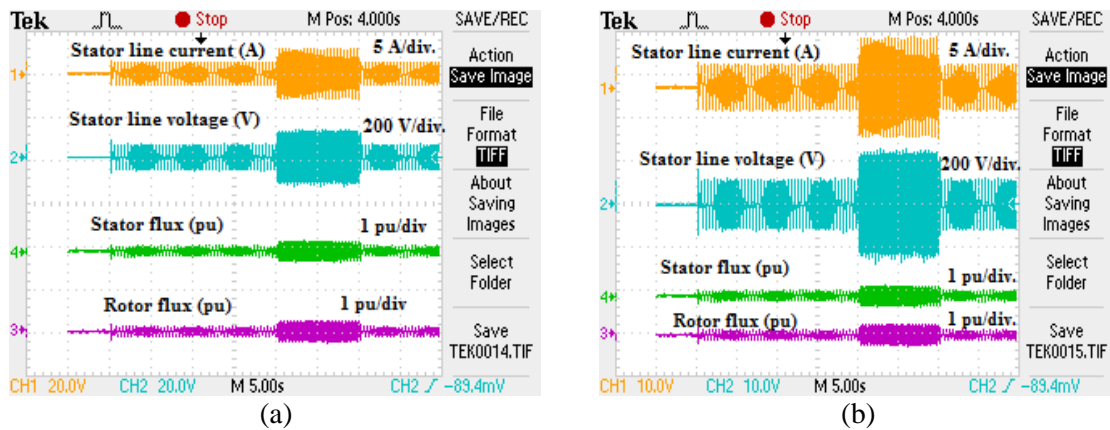


Fig. 10 Comparison of waveforms of stator line current (Channel 1) and voltage (Channel 2), stator flux (Channel 4) & rotor flux (Channel 3) using (a) PIC and (b) NNC based SVM-DTC

Kintex-7 FPGA) processor able to interchange data using a peripheral interface. This processor contains sixty digital Input/output channels to read input signals, forty-eight analog Input/output channels, and a two-channel serial port to read the speed and torque signals of the machine. SEDC motor acts as the prime mover and is attached to a 5.4 HP slip ring induction machine. Power is fed to the machine using one of the inverter modules of a wind emulator; the machine line currents were measured by Hall effects based current sensors and three voltages are measured by LEM LV25-P type of voltage sensors. An incremental optical encoder HEDS 5645 having 512 encoder lines per revolution is employed to measure the actual speed of machine.

6.2 Speed response of generator during variable wind speed

Initially, the wind generator is started with a set speed of 1.024 pu, at this set speed as illustrated Fig. 9 (a) and (b) in channel 1 for both PIC and NNC based DTC methods the speed

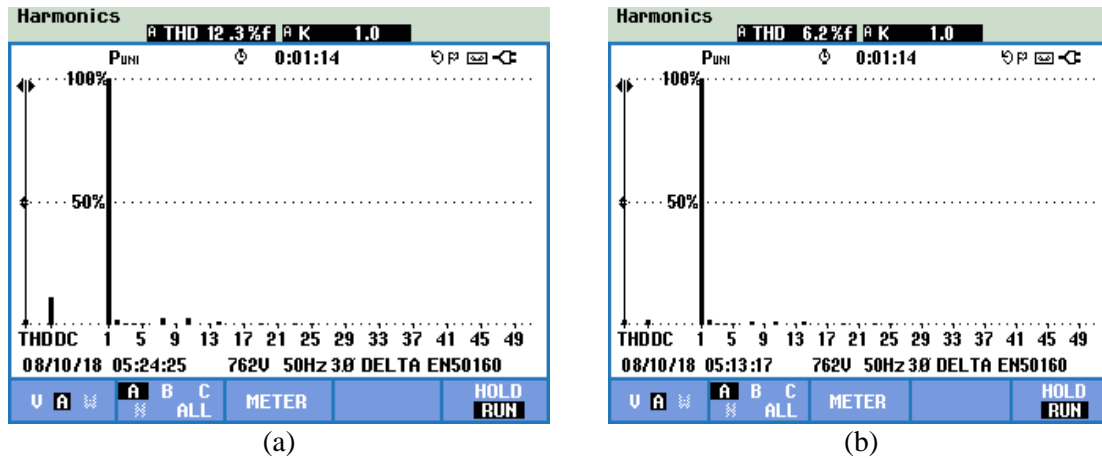


Fig. 11 THD % of stator current using (a) PIC and (b) NNC based SVM-DTC

obtained are 1.031 pu & 1.021 pu respectively. Therefore, using NNC based DTC the speed of the generator is very nearer to the set speed. When wind speed is varied to 13 m/s from 9 m/s at time $t = 2$ s, the peak overshoot and settling time to settle at set speed are 11%, 0.50s and 10 %, 0.40 s respectively for PIC and DTC based DTC method. With wind speed varied to 9 m/s from 13 m/s at time $t = 3$ s, the peak overshoot and settling time to settle at set speed are 12%, 0.59s and 11 %, 0.44 s respectively for PIC and DTC based DTC method. Therefore, implementing NNC in DTC with SVM gives better results compared to PIC based DTC method for DFIG based wind energy system with quicker transient & steady state.

6.3 Active power plot during variable wind speed

Fig. 9 illustrates the real power variation during wind speed variation at channel 2. When the wind speed is 13 m/s, the active power peak goes up to 355 W with PI controller and settles at 0.75 s, whereas the using proposed NNC the peak reaches up to 200 W and settles at 0.6 s. When the wind speed is reduced to 9 m/s, using PI controller the active power varies up to 240 W and settles at 0.60 s, but with NNC based method peak value is 150 W with a lesser settling time of 0.51 s.

6.4 Reactive power plot during wind speed variation

During variable speed variations from 9 m/s to 13 m/s the variation of reactive power is recorded in channel 3 of the oscilloscope. From Fig. 9 during variable speed operations, the reactive power injects into the system is less with NNC based scheme compared to the PIC based rotor side converter control system. During variable speed operation due to weights adjustments and neuron computation of NNC the power injected into the system is reduced. Therefore, from illustrated waveform, it is concluded as reactive power variation using NNC is better than PIC in the context of settling time and oscillation.

6.5 Electromagnetic torque response during variable wind speed

Variations of electromagnetic torque during varying wind speed operations are recorded in

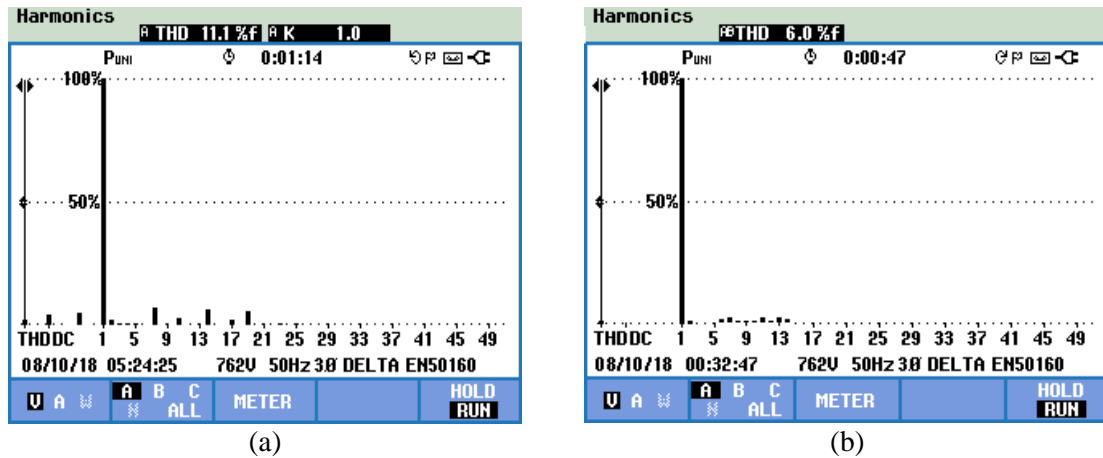


Fig. 12 THD % of stator voltage using (a) PIC and (b) NNC based SVM-DTC

channel 4 of the oscilloscope as illustrated in Fig.9 When speed is changed from 9 m/s to 13 m/s at time $t = 2$ s, from the torque response in terms of undershoot & settling time are 10.8 % & 0.67 s for PIC based SVM DTC whereas for proposed NNC based DTC they are 9.8 % & 0.53 s. Similarly, when the wind speed 13 m/s to 9 m/s, the torque variation is plotted and yields a better response with NNC based DTC method.

6.6 Stator current & voltage variation during change in wind speed

The variation of stator current during variable speed operation is recorded at channel 1 of the oscilloscope as illustrated in Fig. 10. The variation of stator current at a wind speed of 9 m/s is 12 A peak to peak value using PIC whereas for NNC based DTC its peak to peak value is 13.2 A. Similarly, at wind speed of 13 m/s the peak to peak for PIC and NNC are 17.2 and 19.4 also PIC based system takes more time to settle down.

The variation of stator voltage during variable speed operation is recorded at channel 2 of the oscilloscope as illustrated in Fig. 10. From the plot when wind speed is 9 m/s, the stator voltage peak to peak value is 424 V for PI controller with more settling time 0.74 s, for the proposed NNC the peak-to-peak value is 442 V with less settling time 0.68 s. Similarly, when speed is speed 13 m/s, the stator voltage peak to peak values are 760 V and 780 V. The variation of stator and rotor flux of the machine for both PIC and NNC based DTC methods are illustrated in Fig.10 at channel 3 and 4 respectively with NNC based method showing better performance. Total harmonics distortion variation of stator current for PIC and NNC based control methods are 12.3 % & 6.2 % respectively as shown in Fig. 11 whereas stator voltage THD for PIC & NNC are 11.1% & 6 % respectively as illustrated in Fig. 12.

7. Conclusions

This paper presents mathematical modelling and stability analysis for rotor side converter fed doubly fed induction generator-based wind energy system. SVM based DTC using a neural network controller independently control the torque and flux of the machine improves the transient

response of the DFIG based wind energy system. The proposed NNC based DTC is simple to implement in wind energy system at various operating conditions. The proposed method is validated its superiority of dynamic performance improvement compared to other methods at different wind speeds. The performance of DFIG during variable speed operating conditions is improved in the aspect of ripple content, overshoot & settling time for an NNC based SVM-DTC. Further experimental results obtained from the prototype model using space DS Microlab box validates the performance.

Acknowledgments

This research did not receive any specific grant from funding agencies in the public, commercial, or not-for-profit sectors.

References

- Abad, G., López, J., Rodríguez, M.A., Marroyo, L. and Iwanski, G. (2011), "Dynamic modeling of the doubly fed induction machine", *Doubly Fed Induct. Machine*, 209-239.
<https://doi.org/10.1002/9781118104965.CH4>
- Ansari, A.A., Aftab, A.A. and Dyanamina, G. (2021), "MATLAB Simulation of FRT Techniques for DFIG-based Wind Farms", *Proceedings of the 2021 International Conference on Control, Automation, Power and Signal Processing (CAPS)*.
- Ansari, A.A. and Dyanamina, G. (2022a), "Comparative analysis of controlling methods for doubly fed induction generator based wind energy system", *Lecture Notes Electr. Eng.*, **852**, 493-507.
https://doi.org/10.1007/978-981-16-9239-0_37/COVER
- Ansari, A.A. and Dyanamina, G. (2022b), "Fault ride-through operation analysis of doubly fed induction generator-based wind energy conversion systems: A comparative review", *Energies*, **15**(21), 8026.
<https://doi.org/10.3390/EN15218026>
- Ansari, A. A., Dyanamina, G. and Ansari, A.A. (2023), "Decoupled control of rotor side power electronic converter for grid connected DFIG based wind energy system", *Proceedings of the 2023 IEEE International Students' Conference on Electrical, Electronics and Computer Science, SCEECS 2023*.
<https://doi.org/10.1109/SCEECS57921.2023.10063093>
- Babaei, M., Atasoy, A., Hajirasouliha, I., Mollaei, S., Jalilkhani, M., Babaei, M., Atasoy, A., Hajirasouliha, I., Mollaei, S. and Jalilkhani, M. (2022), "Numerical solution of beam equation using neural networks and evolutionary optimization tools", *Adv. Comput. Des.*, **7**(1), 1. <https://doi.org/10.12989/ACD.2022.7.1.001>
- Benbouhenni, H. and Bizon, N. (2021), "Improved rotor flux and torque control based on the third-order sliding mode scheme applied to the asynchronous generator for the single-rotor wind turbine", *Mathematics*, **9**(18), 2297. <https://doi.org/10.3390/MATH9182297>
- Conchas, R.F., Sanchez, E.N., Ricalde, L.J., Alvarez, J.G. and Alanis, A.Y. (2023), "Sensor fault-tolerant control for a doubly fed induction generator in a smart grid", *Eng. Appl. Artif. Intell.*, **117**, 105527.
<https://doi.org/10.1016/J.ENGAPPAI.2022.105527>
- Global wind report (2022), Global wind report 2022; Global Wind Energy Council, GWEC Europe Office – Rue de Commerce 31 1000 Brussels, Belgium. <https://gwec.net/global-wind-report-2022/#data>
- Gupta, R. and Dyanamina, G. (2019), "Matlab simulation of DTC-SVM of doubly fed induction generator for wind energy system", *Proceedings of the 2019 Innovations in Power and Advanced Computing Technologies, i-PACT 2019*. <https://doi.org/10.1109/I-PACT44901.2019.8959990>
- Jaladi, K.K. and Sandhu, K.S. (2018), "DC-link transient improvement of SMC-based hybrid control of DFIG-WES under asymmetrical grid faults", *Int. Transact. Electr. Energy Syst.*, **28**(12), e2633.

- <https://doi.org/10.1002/ETEP.2633>
- Mohammadi, J., Vaez-Zadeh, S., Ebrahimzadeh, E. and Blaabjerg, F. (2018), "Combined control method for grid-side converter of doubly fed induction generator based wind energy conversion systems", *IET Renew. Power Gener.*, **12**(8), 943-952. <https://doi.org/10.1049/IET-RPG.2017.0539/CITE/REFWORKS>
- Mossa, M.A., Saad Al-Sumaiti, A., Duc Do, T. and Zaki Diab, A.A. (2019), "Cost-effective predictive flux control for a sensorless doubly fed induction generator", *IEEE Access*, **7**, 172606-172627. <https://doi.org/10.1109/ACCESS.2019.2951361>
- Muyeen, S.M., Takahashi, R., Murata, T. and Tamura, J. (2009), "A variable speed wind turbine control strategy to meet wind farm grid code requirements", *IEEE T. Power Syst.*, **25**(1), 331-340.
- Nguyen, A.T. and Lee, D.C. (2022), "Sensorless control of variable-speed SCIG wind energy conversion systems based on rotor flux estimation using ROGI-FLL", *IEEE J. Emerg. Select. Topics Power Electron.*, **10**(6), 7786-7796. <https://doi.org/10.1109/JESTPE.2022.3207904>
- Patel, R.K. and Dyanamina, G. (2017), "Direct torque control of doubly fed induction generator for wind energy conversion system", *Proceedings of the 8th International Conference on Computing, Communications and Networking Technologies, ICCCNT 2017*. <https://doi.org/10.1109/ICCCNT.2017.8204050>
- Pena, R., Clare, J.C. and Asher, G.M. (1996), "Doubly fed induction generator using back-to-back PWM converters and its application to variable speed wind-energy generation", *IEEE Proceedings: Electric Power Applications*, **143**(3), 231-241. <https://doi.org/10.1049/IP-EPA:19960288>
- Sahri, Y., Tamalouzt, S., Hamoudi, F., Belaid, S.L., Bajaj, M., Alharthi, M.M., Alzaidi, M.S. and Ghoneim, S.S.M. (2021), "New intelligent direct power control of DFIG-based wind conversion system by using machine learning under variations of all operating and compensation modes", *Energy Reports*, **7**, 6394-6412. <https://doi.org/10.1016/J.EGYR.2021.09.075>
- Squarezi Filho, A.J. (2022), *Model Predictive Control for Doubly-Fed Induction Generators and Three-Phase Power Converters*, Elsevier. <https://doi.org/10.1016/B978-0-32-390964-8.00002-6>
- Takahashi, I. and Noguchi, T. (1986), "A new quick-response and high-efficiency control strategy of an induction motor", *IEEE T. Ind. Appl.*, **22**(5), 820-827. <https://doi.org/10.1109/TIA.1986.4504799>
- Yamasu, V., Wu, B., Sen, P.C., Kouro, S. and Narimani, M. (2015), "High-power wind energy conversion systems: State-of-the-art and emerging technologies", *Proceedings of the IEEE*, **103**(5), 740-788. <https://doi.org/10.1109/JPROC.2014.2378692>
- Zheng, Z., Xie, Q., Huang, C., Xiao, X. and Li, C. (2021), "Superconducting technology based fault ride through strategy for PMSG-based wind turbine generator: A comprehensive review", *IEEE T. Appl. Superconduct.*, **31**(8). <https://doi.org/10.1109/TASC.2021.3101767>